

Measurement of Neutrino Oscillations with the MINOS Detectors in the NuMI Beam

P. Adamson,⁹ C. Andreopoulos,²² K. E. Arms,¹⁸ R. Armstrong,¹² D. J. Auty,²⁶ D. S. Ayres,¹ B. Baller,⁹
P. D. Barnes Jr.,¹⁶ G. Barr,²⁰ W. L. Barrett,³¹ B. R. Becker,¹⁸ A. Belias,²² R. H. Bernstein,⁹ D. Bhattacharya,²¹
M. Bishai,⁴ A. Blake,⁶ G. J. Bock,⁹ J. Boehm,¹⁰ D. J. Boehnlein,⁹ D. Bogert,⁹ C. Bower,¹² E. Buckley-Geer,⁹
S. Cavanaugh,¹⁰ J. D. Chapman,⁶ D. Cherdack,²⁹ S. Childress,⁹ B. C. Choudhary,⁹ J. H. Cobb,²⁰ S. J. Coleman,³²
A. J. Culling,⁶ J. K. de Jong,¹¹ M. Dierckxsens,⁴ M. V. Diwan,⁴ M. Dorman,^{17,22} S. A. Dytman,²¹ C. O. Escobar,⁷
J. J. Evans,^{17,20} E. Falk Harris,²⁶ G. J. Feldman,¹⁰ M. V. Frohne,³ H. R. Gallagher,²⁹ A. Godley,²⁴
M. C. Goodman,¹ P. Gouffon,²³ R. Gran,¹⁹ E. W. Grashorn,¹⁸ N. Grossman,⁹ K. Grzelak,^{30,20} A. Habig,¹⁹
D. Harris,⁹ P. G. Harris,²⁶ J. Hartnell,^{26,22} R. Hatcher,⁹ K. Heller,¹⁸ A. Himmel,⁵ A. Holin,¹⁷ J. Hylen,⁹
G. M. Irwin,²⁵ M. Ishitsuka,¹² D. E. Jaffe,⁴ C. James,⁹ D. Jensen,⁹ T. Kafka,²⁹ S. M. S. Kasahara,¹⁸
J. J. Kim,²⁴ M. S. Kim,²¹ G. Koizumi,⁹ S. Kopp,²⁸ M. Kordosky,^{32,17} D. J. Koskinen,¹⁷ S. K. Kotelnikov,¹⁵
A. Kreymer,⁹ S. Kumaratunga,¹⁸ K. Lang,²⁸ J. Ling,²⁴ P. J. Litchfield,¹⁸ R. P. Litchfield,²⁰ L. Loiacono,²⁸
P. Lucas,⁹ J. Ma,²⁸ W. A. Mann,²⁹ A. Marchionni,⁹ M. L. Marshak,¹⁸ J. S. Marshall,⁶ N. Mayer,¹²
A. M. McGowan,^{1,18} J. R. Meier,¹⁸ G. I. Merzon,¹⁵ M. D. Messier,¹² C. J. Metelko,²² D. G. Michael,^{5,*}
J. L. Miller,^{14,*} W. H. Miller,¹⁸ S. R. Mishra,²⁴ C. D. Moore,⁹ J. Morfin,⁹ L. Mualem,⁵ S. Mufson,¹²
S. Murgia,²⁵ J. Musser,¹² D. Naples,²¹ J. K. Nelson,³² H. B. Newman,⁵ R. J. Nichol,¹⁷ T. C. Nicholls,²²
J. P. Ochoa-Ricoux,⁵ W. P. Oliver,²⁹ R. Ospanov,²⁸ J. Paley,¹² V. Paolone,²¹ A. Para,⁹ T. Patzak,⁸ Ž. Pavlović,²⁸
G. Pawloski,²⁵ G. F. Pearce,²² C. W. Peck,⁵ E. A. Peterson,¹⁸ D. A. Petyt,¹⁸ R. Pittam,²⁰ R. K. Plunkett,⁹
A. Rahaman,²⁴ R. A. Rameika,⁹ T. M. Raufer,²² B. Rebel,⁹ J. Reichenbacher,¹ P. A. Rodrigues,²⁰
C. Rosenfeld,²⁴ H. A. Rubin,¹¹ K. Ruddick,¹⁸ V. A. Ryabov,¹⁵ M. C. Sanchez,^{1,10} N. Saoulidou,⁹ J. Schneps,²⁹
P. Schreiner,³ S.-M. Seun,¹⁰ P. Shanahan,⁹ W. Smart,⁹ C. Smith,¹⁷ A. Sousa,²⁰ B. Speakman,¹⁸ P. Stamoulis,²
M. Strait,¹⁸ P. Symes,²⁶ N. Tagg,²⁹ R. L. Talaga,¹ M. A. Tavera,²⁶ J. Thomas,¹⁷ J. Thompson,^{21,*}
M. A. Thomson,⁶ J. L. Thron,¹ G. Tinti,²⁰ I. Trostin,¹³ V. A. Tsarev,¹⁵ G. Tzanakos,² J. Urheim,¹²
P. Vahle,^{32,17} B. Viren,⁴ C. P. Ward,⁶ D. R. Ward,⁶ M. Watabe,²⁷ A. Weber,²⁰ R. C. Webb,²⁷ A. Wehmann,⁹
N. West,²⁰ C. White,¹¹ S. G. Wojcicki,²⁵ D. M. Wright,¹⁶ T. Yang,²⁵ M. Zois,² K. Zhang,⁴ and R. Zwaska⁹

(The MINOS Collaboration)

¹Argonne National Laboratory, Argonne, Illinois 60439, USA

²Department of Physics, University of Athens, GR-15771 Athens, Greece

³Physics Department, Benedictine University, Lisle, Illinois 60532, USA

⁴Brookhaven National Laboratory, Upton, New York 11973, USA

⁵Lauritsen Laboratory, California Institute of Technology, Pasadena, California 91125, USA

⁶Cavendish Laboratory, University of Cambridge, Madingley Road, Cambridge CB3 0HE, United Kingdom

⁷Universidade Estadual de Campinas, IF-UNICAMP, CP 6165, 13083-970, Campinas, SP, Brazil

⁸APC – Université Paris 7 Denis Diderot, 10, rue Alice Domon et Léonie Duquet, F-75205 Paris Cedex 13, France

⁹Fermi National Accelerator Laboratory, Batavia, Illinois 60510, USA

¹⁰Department of Physics, Harvard University, Cambridge, Massachusetts 02138, USA

¹¹Physics Division, Illinois Institute of Technology, Chicago, Illinois 60616, USA

¹²Indiana University, Bloomington, Indiana 47405, USA

¹³High Energy Experimental Physics Department, ITEP, 117218 Moscow, Russia

¹⁴Physics Department, James Madison University, Harrisonburg, Virginia 22807, USA

¹⁵Nuclear Physics Department, Lebedev Physical Institute, Leninsky Prospect 53, 119991 Moscow, Russia

¹⁶Lawrence Livermore National Laboratory, Livermore, California 94550, USA

¹⁷Department of Physics and Astronomy, University College London, Gower Street, London WC1E 6BT, United Kingdom

¹⁸University of Minnesota, Minneapolis, Minnesota 55455, USA

¹⁹Department of Physics, University of Minnesota – Duluth, Duluth, Minnesota 55812, USA

²⁰Subdepartment of Particle Physics, University of Oxford, Oxford OX1 3RH, United Kingdom

²¹Department of Physics and Astronomy, University of Pittsburgh, Pittsburgh, Pennsylvania 15260, USA

²²Rutherford Appleton Laboratory, Chilton, Didcot, Oxfordshire, OX11 0QX, United Kingdom

²³Instituto de Física, Universidade de São Paulo, CP 66318, 05315-970, São Paulo, SP, Brazil

²⁴Department of Physics and Astronomy, University of South Carolina, Columbia, South Carolina 29208, USA

²⁵Department of Physics, Stanford University, Stanford, California 94305, USA

²⁶Department of Physics and Astronomy, University of Sussex, Falmer, Brighton BN1 9QH, United Kingdom

²⁷Physics Department, Texas A&M University, College Station, Texas 77843, USA

²⁸Department of Physics, University of Texas, 1 University Station C1600, Austin, Texas 78712, USA

²⁹Physics Department, Tufts University, Medford, Massachusetts 02155, USA

³⁰*Department of Physics, Warsaw University, PL-00-681 Warsaw, Poland*

³¹*Physics Department, Western Washington University, Bellingham, Washington 98225, USA*

³²*Department of Physics, College of William & Mary, Williamsburg, Virginia 23187, USA*

This letter reports new results from the MINOS experiment based on a two-year exposure to muon neutrinos from the Fermilab NuMI beam. Our data are consistent with quantum mechanical oscillations of neutrino flavor with mass splitting $|\Delta m^2| = (2.43 \pm 0.13) \times 10^{-3} \text{ eV}^2$ (68% confidence level) and mixing angle $\sin^2(2\theta) > 0.90$ (90% confidence level). Our data disfavor two alternative explanations for the disappearance of neutrinos in flight, namely neutrino decays into lighter particles and quantum decoherence of neutrinos, at the 3.7 and 5.7 standard deviation levels, respectively.

PACS numbers: 14.60.Lm, 14.60.Pq, 29.27.-a, 29.30.-h

Several experiments [1] have produced compelling evidence of the disappearance of neutrinos of a given lepton flavor. In previous publications [2], the MINOS experiment has also presented evidence for energy-dependent disappearance of muon neutrinos produced by the NuMI facility at Fermilab. Based on the number of events, that result provides evidence of the disappearance of ν_μ at a level of 5.2 standard deviations. Such observations support the description of neutrinos via two independent basis sets, the mass and the flavor eigenstates, with the bases related by the 3×3 PMNS matrix [3]. They imply that at least two of the neutrino eigenstates have non-zero mass. In this letter we present results obtained from a larger dataset than that used in [2]. These results provide a precision measurement of the oscillation parameters and further disfavor two other theoretical interpretations of neutrino flavor disappearance [4, 5].

The MINOS detectors [6] and the NuMI beam line [7] are described elsewhere. In brief, NuMI is a conventional two-horn-focused neutrino beam with a 675 m long decay tunnel. The horn current and position of the hadron production target relative to the horns can be configured to produce different ν_μ energy spectra. MINOS consists of two detectors: a 0.98 kt Near Detector (ND) 1.04 km from the NuMI target; and a 5.4 kt Far Detector (FD) 735 km from the target. Both are segmented, magnetized calorimeters that permit particle tracking. The curvature of muons produced in $\nu_\mu + \text{Fe} \rightarrow \mu^- + X$ interactions [19] is used for energy determination of muons that exit the detector and to distinguish the ν_μ component of the beam from the 6% intrinsic $\bar{\nu}_\mu$ contamination. The energy of muons contained in the detector is measured via their range. Oscillations of ν_μ into other neutrino flavors result in an energy-dependent depletion of ν_μ interactions in the FD relative to the expectation based upon the ND measurement.

The present letter describes results from data recorded between May 2005, and July 2007. Over this period, a total of 3.36×10^{20} protons on target (POT) were accumulated for this analysis. A 1.27×10^{20} POT subset of this exposure (hereafter referred to as Run I) forms the data set from Ref [2]. In Run I and for most of the new running period (Run II), the beam line was configured to enhance ν_μ production with energies 1-5 GeV (the low-

energy configuration). An exposure of 0.15×10^{20} POT was accumulated with the beam line configured to enhance the ν_μ energy spectrum at 5-10 GeV (the high-energy configuration). The Run II data were collected with a replacement target of identical construction due to failure of the motion system of the first target. The new target was found to be displaced longitudinally ~ 1 cm relative to the first target, resulting in a 30 MeV shift in the neutrino spectrum. This effect is incorporated in the Monte Carlo simulation, and the Run I and Run II data sets are analyzed separately to account for this shift.

The simulation of neutrino production and detection is accomplished with a model of hadron production in the target using FLUKA [8] and a GEANT3 [9] simulation of the beamline and detector. NEUGEN3.5.5 [10], tuned to data from previous bubble chamber neutrino experiments and experiments with pion beams scattering on iron, is used to model neutrino interactions. As in our previous analysis, the Monte Carlo (MC) simulation of the neutrino flux was constrained to agree with the neutrino energy spectrum in the ND collected in nine different configurations of the NuMI beam [2], thereby reducing uncertainties in the flux prediction at the FD. Fig. 1 compares the simulation to the ND data acquired in the two configurations used in the oscillation analysis.

Neutrino interactions in the MINOS detectors can either be charged-current, $\nu_\mu + \text{Fe} \rightarrow \mu^- + X$, or neutral-current, $\nu_\mu + \text{Fe} \rightarrow \nu_\mu + X$. In this analysis, only the former are used because they identify the interacting neutrino flavor and because the reconstructed energy best measures the full neutrino energy. To select charged-current events, we have implemented a new algorithm [11] based on a multivariate likelihood including four variables that characterize a muon track: the event length; the average pulse height per plane along the track; the transverse energy deposition profile of the track; and the fluctuation of the energy deposited in scintillator strips along the track. The new selection algorithm, along with a new track-finding algorithm, improve our efficiency to identify and select charged-current interactions in the FD from 75.3% using the previous selection [2] to 81.5% in the current selection, in the absence of oscillations. The new selection reduces the neutral-current contamination in the charged-current sample from 1.8% in our previous

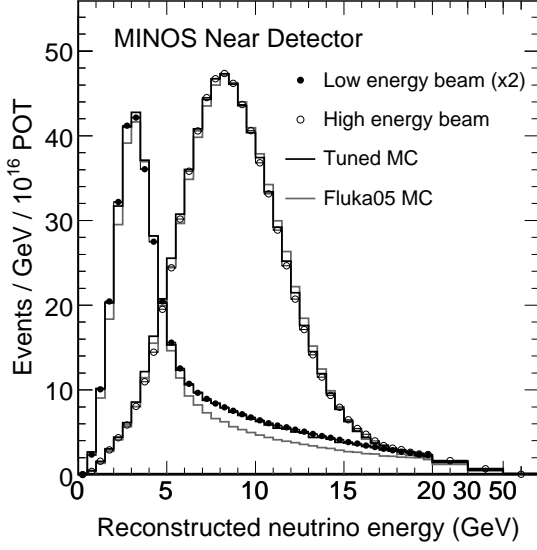


FIG. 1: Energy spectra in the MINOS ND for two of the nine beam configurations before and after tuning the Monte Carlo simulation to the ND data. The data combine Run I + Run II. Both configurations are utilized in the oscillation analysis.

publication to 0.6% in the present analysis. The present analysis uses a larger fiducial mass of 4.17 kt in the FD, an increase of 2.9% over the mass used in [2].

The measured energy spectrum at the ND is used to predict the energy spectrum at the FD. As in our previous analysis [2], we compute a transfer matrix to correct for $\sim 20\%$ differences expected in the shape of the energy spectrum in the FD relative to the ND that arise from meson decay kinematics and from beam-line geometry [2, 12]. We have cross-checked this technique by comparison to other calculations of the FD spectrum [2].

The FD energy spectra were inspected only after the analysis procedure was finalized and basic data integrity checks were performed. We observe 848 events in the FD for all energies 0-120 GeV produced by the NuMI beam, compared to the unoscillated expectation of 1065 ± 60 (syst.). In the low energy configuration alone, the number of events observed in the data is 730, to be compared with an expectation of 936 ± 53 (syst.). The observed energy spectrum of the events from the low- and high-energy datasets is shown along with the predicted spectrum in Fig. 2 and the ratio of these data to the expected spectrum is shown in Fig. 3.

Under the assumption the observed deficit is due to $\nu_\mu \rightarrow \nu_\tau$ oscillations [1], a fit is performed to extract the parameters $|\Delta m^2|$ and $\sin^2(2\theta)$ [13] using the expression

$$P(\nu_\mu \rightarrow \nu_\mu) = 1 - \sin^2(2\theta) \sin^2 \left(1.27 \Delta m^2 \frac{L}{E} \right), \quad (1)$$

where $L[\text{km}]$ is the distance from the target, $E[\text{GeV}]$ is the neutrino energy, and $|\Delta m^2|$ is measured in eV^2 . The FD data from Run I, Run II, and the high-energy run are separately fit to Eq. 1. The best-fit parameters minimize

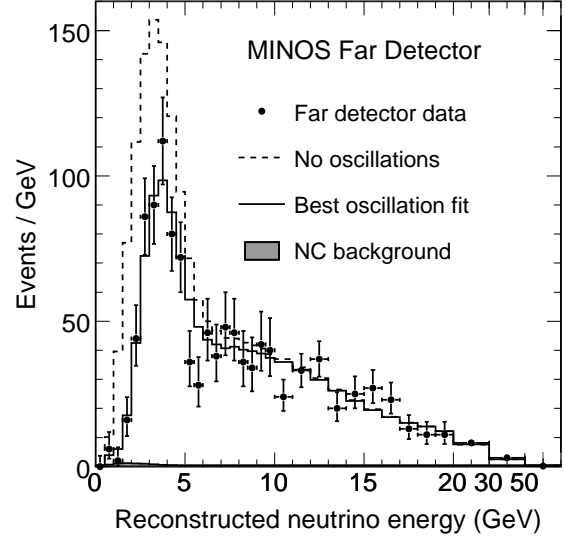


FIG. 2: Comparison of the FD data (points, with statistical uncertainties) from the low- and high-energy configurations with the predictions for the ν_μ energy spectra with and without the effect of oscillations. The estimated neutral current (NC) background is indicated.

the χ^2 expression given in [2]. The predicted oscillated spectrum includes the contamination from ν_τ produced in the oscillation process.

The effects of systematic uncertainties were evaluated by fitting modified MC in place of data. Table I gives the differences between the fitted values obtained with the modified and unmodified MC. The largest effects are: (a) the $\pm 10.3\%$ uncertainty in the absolute hadronic energy scale, which is the sum in quadrature of a $\pm 5.7\%$ error in the calorimeter response to hadrons as derived from test beam measurements [14], a $\pm 2.3\%$ uncertainty in the energy scale calibration, and a $\pm 8.2\%$ uncertainty in the simulation of neutrino production of hadrons in iron nuclei; (b) the $\pm 3.3\%$ relative uncertainty in the hadronic energy scale between the ND and FD; (c) the $\pm 4.0\%$ uncertainty on the predicted FD event rate which is the sum in quadrature of the uncertainties on the detectors' fiducial mass, event selection efficiency and the POT counting; (d) the $\pm 50\%$ uncertainty on the neutral current contamination in the charged current event sample; and (e) the uncertainty on the muon momenta measured via range ($\pm 2.0\%$) or curvature ($\pm 3.0\%$).

In fitting the data to Eq. 1, $\sin^2(2\theta)$ was constrained to lie in the physical region. To reduce the effect of the dominant systematic uncertainties in Table I ((a) and (c) for $|\Delta m^2|$, and (d) for $\sin^2(2\theta)$) these three systematic uncertainties were included as nuisance parameters in the fit. The resulting best fit to the neutrino energy spectrum is shown in Fig. 2 and Fig. 3. We obtain $|\Delta m^2| = (2.43 \pm 0.13) \times 10^{-3} \text{ eV}^2$ and $\sin^2(2\theta) > 0.95$ at 68% confidence level (C.L.) [15]. The fit $\chi^2 = 90$ for 97 degrees of freedom. The resulting 68% C.L. ($\Delta\chi^2 = 2.30$)

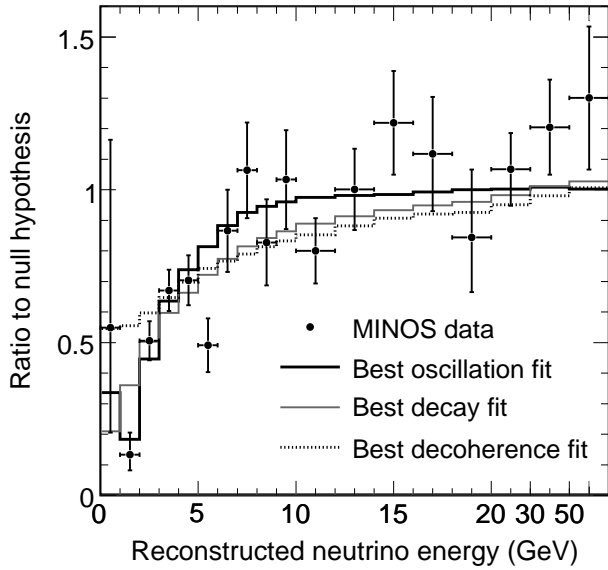


FIG. 3: Ratio of the FD data and the expected spectrum in the absence of oscillations. Also shown are the best fit curve to Eq. 1 and the best fit to alternative models of neutrino disappearance [4, 5]. For display purposes, the data have been rebinned and the estimated oscillated NC background is subtracted.

Uncertainty	$ \Delta m^2 $ (10^{-3} eV^2)	$\sin^2(2\theta)$
(a) Abs hadronic E scale ($\pm 10.3\%$)	0.052	0.004
(b) Rel hadronic E scale ($\pm 3.3\%$)	0.027	0.006
(c) Normalization ($\pm 4\%$)	0.081	0.001
(d) NC contamination ($\pm 50\%$)	0.021	0.016
(e) μ momentum (range 2%, curv 3%)	0.032	0.003
(f) $\sigma_\nu(E_\nu < 10 \text{ GeV})$ ($\pm 12\%$)	0.006	0.004
(g) Beam flux	0.010	0.000
Total Systematic Uncertainty	0.108	0.018
Expected Statistical Uncertainty	0.19	0.09

TABLE I: Sources of systematic uncertainties in the measurement of $|\Delta m^2|$ and $\sin^2(2\theta)$. The values are the average shifts for varying the parameters in both directions without imposing the $\sin^2(2\theta) \leq 1$ constraint on the fit. Correlations between the systematic effects are not taken into account. The dominant uncertainties are incorporated as nuisance parameters in the fit of our data to Eq. 1 so as to reduce their effect on the oscillation parameter measurement (see text).

and 90% C.L. ($\Delta\chi^2=4.61$) intervals for the oscillation parameters $|\Delta m^2|$ and $\sin^2(2\theta)$ are shown in Fig. 4 [16]. The MC predicts negligible backgrounds of 0.7 events from cosmic ray muons, and, at the best-fit value for $|\Delta m^2|$ and $\sin^2(2\theta)$, 2.3 events from neutrino interactions in the upstream rock, 5.9 neutral current and 1.5 ν_τ events in the final sample. If the fit is not constrained to the physical region, $|\Delta m^2|=2.33 \times 10^{-3} \text{ eV}^2$ and $\sin^2(2\theta)=1.07$, with a 0.6 unit decrease in χ^2 . Correspondingly, the contours in Fig. 4 are smaller than those expected for the

present data set. Our measurement is the most precise determination of the mass splitting $|\Delta m^2|$.

Fig. 4 also shows that the previous MINOS result [2] is in good agreement with the current measurement. Taken alone, the Run II data yield $|\Delta m^2|=(2.32^{+0.17}_{-0.16}) \times 10^{-3} \text{ eV}^2$ and $\sin^2(2\theta)=1.0$, to be compared with $(2.57^{+0.23}_{-0.20}) \times 10^{-3} \text{ eV}^2$ and $\sin^2(2\theta)=1.0$ from Run I. The two results are consistent at 68% C.L. We note that the value of $2.57 \times 10^{-3} \text{ eV}^2$ for Run I differs from that quoted in [2] because of our improved reconstruction and selection of charged-current events and improved MC simulation of neutrino interactions.

We have also fit the FD energy spectra to alternative models that have been proposed to explain the disappearance of neutrinos in flight, namely, the decay of neutrinos to lighter particles (Eq. 13 of [4]), and the decoherence of the neutrino's quantum-mechanical wave packet (Eq. 5 of [5]). Fig. 3 shows the ratios of the energy spectra arising from our best fits to these alternative models to the prediction of the FD spectrum in the absence of ν_μ disappearance. The χ^2 for the best fit to the decay model is 104/97 d.o.f., while that for the decoherence model is 123/97 d.o.f. Given the $\Delta\chi^2 = 14$ and 33 of these two models relative to the oscillation hypothesis, these models are disfavored with respect to the oscillation hypothesis at the 3.7 and 5.7 standard-deviation levels.

In summary, we have presented updated measurements of neutrino oscillation parameters from the MINOS experiment. Based upon an exposure of 3.36×10^{20} POT from the NuMI beam, we obtain $|\Delta m^2| = (2.43 \pm 0.13) \times 10^{-3} \text{ eV}^2$ (68% C.L.) and mixing angle $\sin^2(2\theta) > 0.90$ (90% C.L.). As the dataset presented here includes the subset analyzed in [2], these results supersede our previous publication. Our data disfavor two alternative explanations for disappearance of neutrinos in flight, namely neutrino decays [4] into lighter particles and quantum decoherence of neutrinos [5] at the 3.7 and 5.7 standard-deviation level, respectively.

This work was supported by the US DOE; the UK STFC; the US NSF; the State and University of Minnesota; the University of Athens, Greece; and Brazil's FAPESP and CNPq. We are grateful to the Minnesota Department of Natural Resources, the crew of the Soudan Underground Laboratory, and the staff of Fermilab for their contribution to this effort.

* Deceased.

- [1] W.-M. Yao *et al.*, J. Phys. G 33, 1 (2006).
- [2] D.G. Michael *et al.*, Phys. Rev. Lett. 97, 191801 (2006); P. Adamson *et al.*, Phys. Rev. D77, 072002 (2008).
- [3] B. Pontecorvo, JETP 34, 172 (1958). Z. Maki, M. Nakagawa, and S. Sakata, Prog. Theor. Phys. 28, 870 (1962).
- [4] V. Barger *et al.*, Phys. Rev. Lett. 82 2640 (1999).
- [5] G. L. Fogli *et al.*, Phys. Rev. D67 093006 (2003).

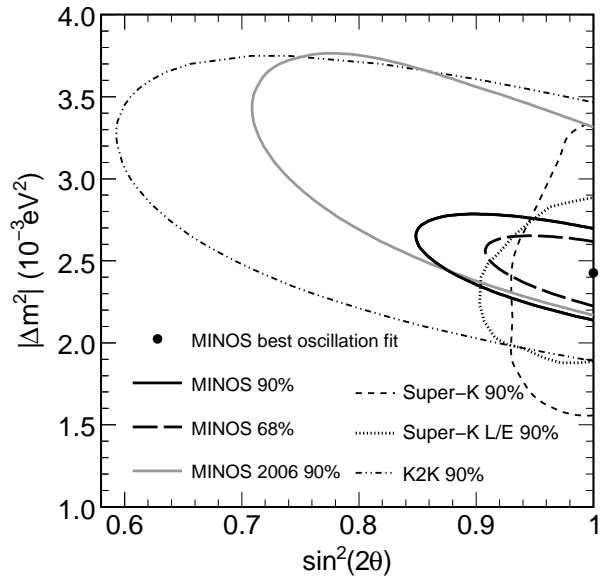


FIG. 4: Contours for the oscillation fit to the data in Fig. 2, including systematic errors. Also shown are contours from previous experiments [17, 18] and our earlier result [2].

- [6] D.G. Michael *et al.*, submitted to Nucl. Instr. and Meth.
 [7] S. Kopp, Proc. 2005 IEEE Part. Accel. Conf., May 2005,

- Fermilab-Conf-05-093-AD and [arXiv:physics/0508001](https://arxiv.org/abs/physics/0508001).
 [8] A. Fasso *et al.*, CERN-2005-10, INFN/TC.05/11, SLAC-R-773 (2005).
 [9] R. Brun *et al.*, CERN Program Library W5013 (1984).
 [10] H. Gallagher, Nucl. Phys. B (Proc. Suppl.) 112, 188 (2002); update at [arXiv:0806.2119](https://arxiv.org/abs/0806.2119) (2008).
 [11] R. Ospanov, PhD Dissertation, UT-Austin, 2008
 [12] M. Szleper and A. Para, hep-ex/0110001.
 [13] The experiment measures an unresolved mixture of $|\Delta m_{31}^2|$ and $|\Delta m_{32}^2|$, which we refer to as $|\Delta m^2|$ for brevity. The parameter $\sin^2(2\theta)$ is likewise an admixture. For further discussion see G. L. Fogli *et al.*, Prog. Part. Nucl. Phys. 57, 742 (2006).
 [14] P. Adamson *et al.*, Nucl. Inst. & Meth. A556, 119 (2006).
 [15] Although the contours in Fig. 4 are calculated with two degrees of freedom (d.o.f.), the parameter errors are calculated with only one d.o.f. as in [1] using $\Delta\chi^2 = 1$ and 2.71, respectively.
 [16] The effect of the constraint to the physical region was investigated using the unified approach of G.J. Feldman and R.D. Cousins, Phys. Rev. D57, 3873, (1998), which gave slightly smaller confidence intervals.
 [17] Y. Ashie *et al.*, Phys. Rev. Lett. 93, 101801 (2004); Phys. Rev. D71, 112005 (2005).
 [18] M.H. Ahn *et al.*, Phys Rev D 74 072003 (2006).
 [19] Approximately 5% of ν_μ interactions occur in aluminum and scintillator.